Sensing short range forces with a nanosphere matter-wave interferometer

Andrew Geraci[*]

Department of Physics, University of Nevada, Reno, Nevada 89557, USA

Hart Goldman[†]

Department of Physics, Stanford University, Stanford, California 94305, USA

We describe a method for sensing short range forces using matter-wave interference in dielectric nanospheres. When compared with atom interferometers, the larger mass of the nanosphere results in reduced wave-packet expansion, enabling investigations of forces nearer to surfaces in a free-fall interferometer. By laser cooling a nanosphere to the ground state of an optical potential and releasing it by turning off the optical trap, acceleration sensing at the 10^{-8} m/s^2 level is possible. The approach can yield improved sensitivity to Yukawa-type deviations from Newtonian gravity at the 5 μm length scale by a factor of 10^4 over current limits.

I. INTRODUCTION

Light-pulse atom interferometers have been demonstrated as a powerful tool for precision sensing, enabling gravimetry at the $10^{-9}g$ level [1–3], gravity gradiometry at the 10^{-9} s$^{-2}/\sqrt{\text{Hz}}$ level [4], and rotation sensing at the 10^{-8} rad/s/$\sqrt{\text{Hz}}$ level [5]. Atom interferometers can also be used in principle for measuring the gravitational attraction of nearby masses [6] and for tests of deviations from Newton's inverse square law of gravitation [7–13]. In addition atom interferometers can be used as a surface probe for electromagnetic forces [14] such as Casimir–Polder forces [15–19]. A challenge for applying light-pulse atom interferometers to such measurements in proximity to surfaces results from the finite wave-packet expansion of the atomic cloud. By replacing the atom with a massive dielectric object which is laser cooled to its motional ground state in an optical trap, the velocity spread dramatically decreases as $(m_\text{a}/M)^{1/2}$, where m_a and M are the mass of the atom and sphere, respectively, enabling measurement times of order 1 s with a wave-packet spread of order 1 μm.

In this paper we describe two protocols which utilize macroscopic matter-wave phenomena in dielectric spheres to perform sensitive acceleration measurements near material surfaces. First we describe a near-field Talbot interferometer [20–22] which diffracts a sphere from a pure phase grating made of light to generate a density distribution with a fringe pattern at twice the grating period. Such a setup can be used as an accelerometer to test for corrections to Newtonian gravity at short range. These corrections are generally parametrized according to a Yukawa-type potential

$$V(r) = -\frac{G_N m_1 m_2}{r}[1 + \alpha e^{-r/\lambda}], \qquad (1)$$

where m_1 and m_2 are two masses interacting at distance r, α is the strength of the potential relative to gravity, and λ is the range of the interaction. For two objects of mass density ρ and linear dimension λ with separation $r \approx \lambda$, a Yukawa force scales roughly as $F_Y \sim G_N \rho^2 \alpha \lambda^4$, decreasing rapidly with smaller λ. We estimate sufficient sensitivity to measure $\alpha = 400$ at the $\lambda = 5$ μm length scale in such a setup. The current experimental limits at 5 μm are $|\alpha| > 3 \times 10^6$ [23]. Thus, an improvement by several orders of magnitude is possible in searches for beyond-the-standard-model physics which can naturally produce large deviations $|\alpha| \gg 1$ at μm-scale distances, including supersymmetry [11], string theory [24,25], and vector or scalar particles residing in large extra dimensions [26,27].

We then compare this to a ballistic experiment which is not based on interference, in which a larger nanosphere is initially cooled to the ground state of an optical potential. After cooling, the optical trap is ramped down quickly allowing the sphere to undergo free wave-packet expansion at a rate determined by the ground state momentum spread. For 200 nm diameter spheres, such an approach has a sensitivity of 1 μGal $= 10^{-8}$ m/s^2, which is comparable to falling corner cube gravimeters [28]. We compare the two techniques as a function of the temperature and mass of the nanosphere and conclude with a discussion of the systematic error and noise sources for each measurement protocol.

II. PROTOCOL

A diagram of the interferometry protocol is given in Fig. 1, and a list of experimental parameters is given in Table I. We consider a silicon sphere of radius $R = 6.5$ nm (and mass $M \approx 1.5 \times 10^6$ amu) which is optically trapped and cooled such that its center-of-mass wave function ψ_{CM} is near the harmonic oscillator ground state with the oscillator frequency ω determined by the trap. Silicon is
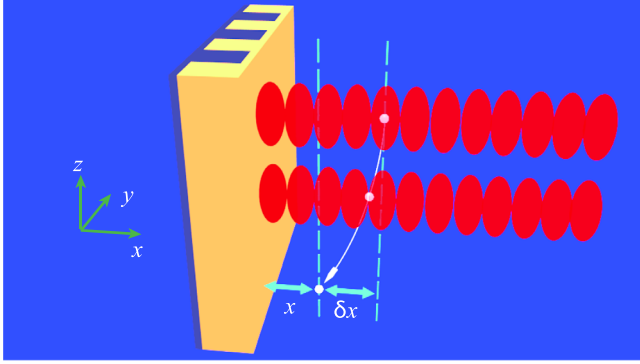
[*]ageraci@unr.edu
[†]hgoldman@stanford.edu

FIG. 1 (color online). Proposed experimental setup. A nano-sphere is cooled in an optical trap and allowed to fall in proximity to a wall which acts as a source mass. After falling for a time T_T, a light pulse grating is applied. After another time T_T, the position of the sphere is recorded. Such measurements combine to reveal an interference pattern, where the node positions depend on the transverse (x) acceleration experienced by the bead throughout its fall. The centroid of the distribution also shifts toward the wall by an amount δx as a result of the acceleration. The wall consists of vertical sections of varying density to modulate the x-component of the gravitational acceleration on the sphere due to the wall, depending on the initial y-position of the trap. By comparing the results of experiments in which the sphere is initially positioned to fall next to a dense (gold) vertical section vs a less dense (silicon) vertical section, searches for Yukawa-type corrections to gravity can be performed at the 5 μm length scale.

chosen for its combination of low-optical absorption and low blackbody emissivity [22]. The sphere is then released from the trap and allowed to fall freely in the z-direction (with the x-direction being transverse to the fall) next to a wall behind which a mass can be placed. Immediately after it is released, the wave function has transverse spread $\sigma_x = \sqrt{\frac{\hbar}{2M\omega}} \approx 6$ nm. After one Talbot time $T_T = Md^2/h$, the wave packet has expanded, and the sphere is diffracted by a pure phase grating of period $d = 0.25$ μm. The size of the sphere is chosen such that $T_T = 0.25$ s.

The sphere is then allowed to propagate a time T_T after the grating to a position-sensitive detector, which can be an optical cavity or split photodetector. For cavity assisted readout of the final displacement of the sphere, the relevant optomechanical coupling which describes the change of the cavity resonance frequency ω_c due to the motion of the

TABLE I. Experimental parameters for the interference protocol corresponding to a total fall time of $2T_T = 0.5$ s.

Parameter	Symbol	Value
Sphere radius	R	6.5 nm
Sphere density	ρ	2300 kg/m^3
Dielectric constant	ϵ	18
Trap frequency	ω	$2\pi \times 100$ Hz
Grating period	d	0.25 μm
Grating peak intensity	I	16 kW/m^2

sphere is given by $\partial\omega_c/\partial z = 2k_L g_s$. Here the coupling strength $g_s = \frac{3V}{4V_c}\frac{\epsilon-1}{\epsilon+2}\omega_c$, where ϵ is the dielectric constant of the sphere of volume V and V_c and $\kappa = \pi c/L\mathcal{F}$ are the cavity mode volume and line width, respectively, and $\mathcal{F}$ is the cavity finesse. For an incident laser with power P_c and frequency ω_c, photon shot noise limits the minimum detectable phase shift to $\delta\phi \approx 1/(2\sqrt{I})$ where $I \equiv P_c/(\hbar\omega_c)$ [29]. The corresponding photon shot-noise limited displacement sensitivity is $\sqrt{S_z(\omega)} = \frac{\kappa}{4k_L g_s}\frac{1}{\sqrt{I}}\sqrt{1 + \frac{4\omega^2}{\kappa^2}}$ [30], along the cavity axis for an impedance matched cavity. For a 532 nm readout laser of 10 mW with a waist 10 μm and $\mathcal{F} = 100$, the displacement sensitivity is 9 pm/$\sqrt{\text{Hz}}$. A split photodetector was recently used to measure the position of a nanosphere with 1.2 pm/$\sqrt{\text{Hz}}$ resolution [31]. We estimate that a position resolution of $\sim$30 pm/$\sqrt{\text{Hz}}$ is adequate for the proposed measurements.

After recording the position of the sphere after several experiments, an interference pattern builds up one measurement at a time, with fringes spatially separated by $2d$. An acceleration a in the transverse direction due to the presence of the wall results in a shift in the fringe pattern by an amount $\delta x_\phi = -aT_T^2$. A measurement of the influence of the gravitational attraction of the mass can then be obtained from the relative phase between the fringe patterns with and without the presence of the mass behind the wall.

The effect of the grating on the wave function can be understood using the phase-space formalism of Ref. [32]. If the sphere is cooled to the ground state of c.m. motion, its initial Wigner function is $w_0(x, p) = A \cdot \exp\left[-\frac{x^2}{\sigma_x^2} - \frac{p^2}{\sigma_p^2}\right]$, where A is fixed by normalization. After falling for a time t with transverse acceleration a, the Wigner distribution is sheared accordingly as $w_1(x, p; t) = w_0(x - \frac{p}{M}t + \frac{1}{2}at^2, p - Mat)$. At the grating, the wave function undergoes a transformation of the form $|\psi_{CM}\rangle \mapsto U|\psi_{CM}\rangle$ [33] (see also the Appendix). Since the de Broglie wavelength of the sphere is small compared with the interaction range of the optical potential, we can employ the eikonal approximation $U(x) = \exp(i\phi(x))$, where $\phi(x) = -\frac{1}{\hbar}\int_{-\infty}^{\infty} V(x,t)dt = \frac{\alpha_\omega I\tau}{\hbar c\epsilon_0}\sin^2(\pi x/d) \equiv \phi_0\sin^2(\pi x/d)$. Here $\alpha_\omega = 4\pi R^3\epsilon_0\left(\frac{\epsilon-1}{\epsilon+2}\right)$ is the polarizability of the sphere, I is the peak laser intensity, and $\tau = 1$ μs is the pulse duration.

After propagating to the grating over a time t_0 and falling for an additional time t_1 from the grating to the detector, the final fringe pattern in the probability density $|\psi_{CM}(x)|^2$ can be obtained by integrating the final Wigner distribution over momentum. A detailed description of the Wigner function evolution is provided in the Appendix. We find an optimum fringe contrast for $\phi_0 \approx 1.5$. The final fringe pattern develops a phase $\Phi(a, t_0, t_1)$ which is proportional to the transverse acceleration a to lowest order: $\Phi(a, t_0, t_1) \approx \left(\frac{i\pi t_0 t_1}{d}\right)a$. For $t_0 = t_1 = T_T$ and $R = 6.5$ nm, the acceleration required for a π phase shift in the fringe
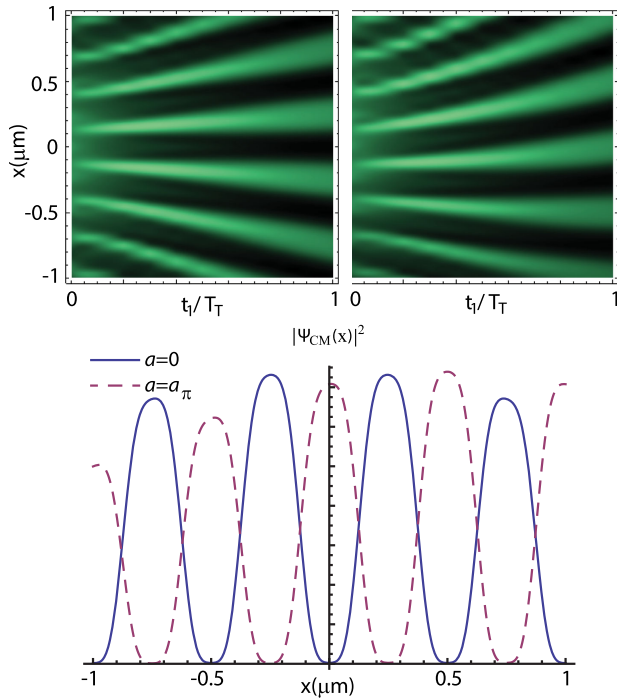
FIG. 2 (color online). (left) Density plot of $|\Psi(x)|^2$ following the grating for zero acceleration for releasing the trap at $\omega_0 = 2\pi \times 100$ Hz from its ground state. (right) As in the left panel, with $a_\pi = 4 \times 10^{-7}g$ constant acceleration. (lower) Line outs taken at $t_1 = T_T$ after the grating for $a = 0$ (solid) and $a = a_\pi$ (dashed).
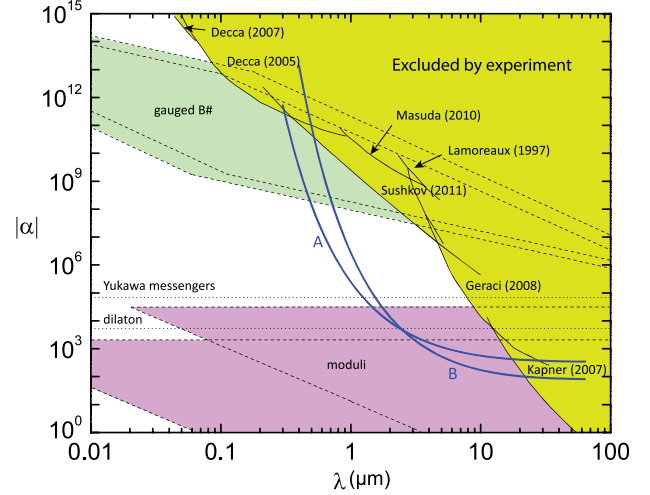

FIG. 3 (color online). Current experimental bounds [23,34–40] and theoretical predictions [7] for a non-Newtonian potential of the form $V(r) = -\frac{G_N m_1 m_2}{r}[1 + \alpha \exp(-\frac{r}{\lambda})]$ between two masses m_1 and m_2 separated by r. Curves A and B are the predicted sensitivities for wall separation 6 and 10 μm, with corresponding Talbot times of 0.1 and 0.25 s, respectively.

pattern is approximately $a_\pi = d/T_T^2 = 4\,\mu\text{m/s}^2 = 4 \times 10^{-7}g$. Thus, the sensitivity of the experiment is determined by the grating period and time of the fall. If the sphere has an initial transverse momentum kick, the phase shift Φ remains the same, which means that, while this experiment is highly sensitive to transverse acceleration, it is insensitive to any systematic initial momentum kicks. Plots of the probability densities we obtain for parameters given in Table I are shown in Fig. 2 for $a = 0$ and $a = a_\pi$.

The above assumes that the sphere can be cooled to its ground state of the c.m. motion. However, it is possible to obtain a fringe pattern at temperatures above that of the ground state, where the c.m. wave function becomes a superposition of harmonic oscillator eigenstates. The effect of the temperature on the Wigner distribution can be approximated as a widening of the position and momentum spreads of the pure ground state distribution according to $k_B T \approx \hbar \omega \bar{n}(T) \approx M\omega^2 \sigma_x^2(T)$, where $\bar{n}(T)$ is the average principal quantum number of the c.m. state at temperature T. Therefore, the position (and momentum) spread grows as $\sqrt{\bar{n}(T)}$ at large T.

A. Short range force measurements

The Casimir–Polder force between a small dielectric sphere and metal plane can be written as [16] $F_{cp} = -\frac{3\hbar c \alpha_\omega}{8\pi^2 \epsilon_0} \frac{1}{z^5}$.

This force results in an acceleration of $4 \times 10^{-7}g$ on the sphere and displaces the fringe pattern by approximately π for a surface separation of 10 μm and $R = 6.5$ nm, $T_T = 0.25$ s. The phase shift is $\approx 3\pi$ for $R = 5$ nm, $T_T = 0.1$ s, and a surface separation of 6 μm. Thus, by averaging over 10^4 shots, the Casimir–Polder acceleration can be measured at or below the percent level. Such measurements may be relevant for the study of the quantum states of nanospheres near surfaces [17].

For a short-distance gravity measurement, we consider the differential shift in the fringe pattern between the case where the sphere falls next to a gold section of the wall and the case where the sphere falls next to a silicon section of the wall. Here the shift from the Casimir acceleration is common to both cases as a 200 nm thick uniform gold coating covers the surface of the wall. We take the width of the gold and silicon sections to be 40 μm. We consider two cases, with $R = 6.5$ nm, $T_T = 0.25$ s, and a 10 μm separation of the sphere from the wall, and with $R = 5$ nm, $T_T = 0.1$ s, and 6 μm sphere-wall separation. The projected sensitivity is shown in Fig. 3 for a phase resolution of $\pi/300$, corresponding to averaging over 10^5 shots of the experiment.

III. COMPARISON OF INTERFERENCE AND BALLISTIC MEASUREMENTS

It is interesting to compare the position sensitivity for a ballistic approach where the position of the sphere is measured after falling from the trap vs the Talbot interferometer sensitivity. Assuming the particle is cooled to the ground state in the harmonic trap, the velocity spread due to

the zero point motion $\sigma_v = \sqrt{\frac{\hbar\omega}{2M}}$ will cause a spread in the measured position of the bead after it falls during the experiment. The position spread after a measurement at time t later is thus given by $\sigma_v t$. After N repeated experiments, the uncertainty in the mean of the distribution goes as $\sigma_v t/\sqrt{N}$. This uncertainty is added to the signal $\delta x = \frac{1}{2}at^2$ for an acceleration a toward the wall. In the Talbot interferometer, the fringe pattern shifts by a comparable amount due to the acceleration from the wall. However, the momentum uncertainty in the ground state harmonic oscillator trap does not influence the location of particular interference fringes—only the overall envelope is influenced by the initial momentum spread. The uncertainty in the fringe position of the fringe maxima when taking N measurements is $\sim d/\sqrt{N}$. Since the period is known, the fringe pattern can be fit using a function with a known period and variable phase. The improvement over the ballistic measurement is given by $\beta = \chi \sigma_v t/d$, where χ is the fringe contrast of the interferometer. Plots of β as a function of mass are given for various temperatures in Fig. 4 for a fixed fall time of $t = 2T_T = 0.5$ s.

At temperatures near the ground state temperature, the increasing mass results in the increasing localization and ultimately a wave packet which is too narrow to interact with the grating, at which point the interference signal vanishes. For higher temperatures, the position and velocity spreads become large enough to let higher masses interact with the grating, but velocity spreads which are large compared to the grating velocity $v_g = \hbar/dM$ result in reduced contrast. Increases in the mass actually improve the sensitivity of the interference setup until one strays too far from the Talbot condition [i.e. $T_T(M) \gg t$]. At this point the contrast of the fringe pattern falls until there is no more visibility. Thus, at higher temperatures, β increases for some mass interval, peaks, and subsequently falls to zero.
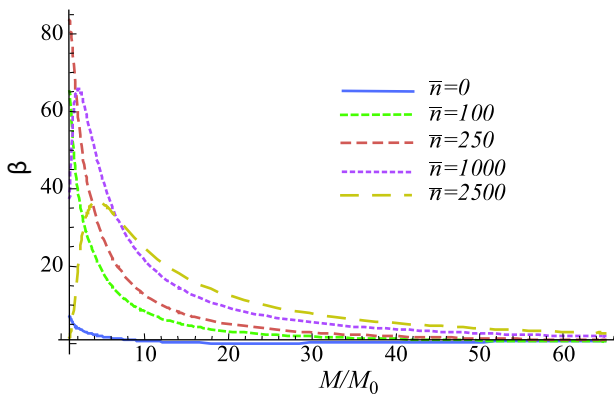

FIG. 4 (color online). The improvement factor β for an interference experiment relative to a ballistic wave-packet expansion experiment as a function of mass at various temperatures. The fall time is fixed at $t = 0.5$ s, corresponding to $2T_T$ for a sphere of mass $M = M_0$, where $M_0 \equiv \frac{4}{3}\rho\pi R^3$ with $R = 6.5$ nm.

If the mass is increased without also extending the time of flight to maintain the Talbot time condition, the ballistic experiment eventually exceeds the sensitivity of the interference experiment, with the caveat that the location of the sphere at the end of the experiment is sensitive to systematic errors in the initial velocity distribution upon release from the optical trap. For a 100 nm radius sphere initially cooled to the ground state and allowed to expand and fall ballistically, the sensitivity curves are approximately 10 times better than those shown in Fig. 3, however, with this additional source of error.

IV. SYSTEMATICS

While the effect of decoherence due to gas collisions is negligible for our setup, Rayleigh scattering of photons from the laser grating can result in decoherence in the interference experiment. The timescale for this, however, can be much larger than $\tau = 1$ μs. Since the spread of the c.m. wave function at the grating is of order $\sim d$, the decoherence time is roughly the time for one scattering event, approximately 2 ms. More significantly, blackbody emission from the sphere as it is falling can result in decoherence. However, the low emissivity of silicon allows for measurements on the time scales we require [22].

A deviation in vertical alignment will produce a constant offset in the measured acceleration. If each shot has a varying misalignment, this becomes an additional noise source. Such noise is negligible for tilt fluctuations of the apparatus of ~ 0.5 μrad$/\sqrt{\text{Hz}}$. While the fringe locations are insensitive to any systematic velocity kick given to the falling sphere as it is released from the optical trap, the setup is sensitive to vibrational noise in the mirrors during the application of the grating pulse and during the detection of the sphere. Maximal sensitivity requires vibrational stability of $\sim 10^{-3}$ μm$/\sqrt{\text{Hz}}$ at frequencies around 1 Hz.

The charge on the dielectric sphere will produce a significant background in the presence of stray electric fields. However, recent experimental work has shown that the charge on optically trapped spheres can be made zero and remain zero for long measurement periods [41,42].

The polycrystalline structure of the gold coating on the wall results in local electric field variations due to the patch effect [43,44]. These patch potentials can drift with time and vary over the spatial extent of the wall. We can estimate the acceleration applied to the sphere as a result of typical patch potentials ranging from ~ 50 mV variations over length scales of a few μm to be of order $10^{-7}g$. Such accelerations will contribute to the fringe shift of the interferometer and would need to be characterized experimentally. However, the initial trap can be translated laterally, so that the experiment can first be performed with the sphere closest to a gold section of the wall, then closest to the adjacent silicon section of the wall, then closest to the next gold section, etc., as shown in Fig. 1. Thus, by scanning the initial y-position of the sphere along

the wall, one expects a spatially periodic signal for the acceleration due to the mass. The variation of the acceleration due to the patch effect is not expected to exhibit the same periodicity as the underlying spatial density pattern in the wall. This can be used in principle to distinguish the effects. For example, assuming random patch variations on the μm scale, the spatial Fourier component of the patch effect at the period of the mass density modulation should be suppressed as $1/\sqrt{N_y}$ for N_y initial y-positions. In this case we roughly expect sensitivity at the $10^{-8}g$ level for $N_y = 100$. The required value of N_y would ultimately need to be determined from the experimentally measured patch variations.

The Casimir–Polder force can also produce a background systematic effect if the screening provided by the uniform gold coating on the wall is not adequate due to its finite thickness and conductivity. This can lead to a differential acceleration for the cases where the sphere is close to a gold section vs silicon section of the wall, despite the uniform metal coating on the surface. Using the method developed in Ref. [45] to determine the finite conductivity and thickness effects, we estimate that for a uniform gold thickness of 200 nm the screening is adequate for measurements at the projected level of sensitivity.

V. DISCUSSION

The matter-wave accelerometer we have presented can be advantageous when compared with light-pulse atom interferometry for use in surface-force measurements where localization of the sensor is required. This technique could lead to advances in tests of inverse-square law violations of gravity at μm distances and Casimir force measurements between nanospheres and surfaces.

ACKNOWLEDGMENTS

APPENDIX: EFFECT OF THE GRATING IN THE WIGNER FUNCTION FORMALISM

The initial state Wigner distribution associated with the sphere's c.m. mode in the $x-$ direction is given as

$$w_0(x, p) = \frac{1}{2\pi\hbar} \int_{-\infty}^{\infty} ds\, e^{isp/\hbar} \langle x - s/2|\hat{\rho}|x + s/2\rangle, \quad \text{(A1)}$$

where $\hat{\rho}$ is the density matrix for the c.m. mode. If the sphere is cooled to the ground state of center-of-mass motion, its initial wave function will be that of a pure quantum harmonic oscillator ground state of position spread σ_x and momentum

spread $\sigma_p = \hbar/\sigma_x$, so $w_0(x, p) = A \cdot \exp\left[-\frac{x^2}{\sigma_x^2} - \frac{p^2}{\sigma_p^2}\right]$, where A is fixed by normalization. After falling for a time t_0, the Wigner distribution is sheared accordingly as $w_1(x, p; t_0) = w_0(x - \frac{p}{M} t_0 + \frac{1}{2} a t_0^2, p - Mat_0)$, where w_0 is the Wigner distribution at time $t = 0$ and a is the acceleration in the x-direction [32]. At the grating, the wave function undergoes a transformation of the form $|\psi_{CM}\rangle \mapsto U|\psi_{CM}\rangle$, so the density matrix transforms as $\rho \mapsto U\rho U^\dagger$. Because the de Broglie wavelength of the sphere is small compared to the range of the grating potential, we may employ the eikonal approximation, in which $U(x) = \exp(i\phi(x))$ and $\phi(x) = -\frac{1}{\hbar}\int_{-\infty}^{\infty} V(x, t)dt = \frac{\alpha_\omega I\tau}{\hbar c\epsilon_0}\sin^2(\pi x/d) \equiv \phi_0\sin^2(\pi x/d)$ is an integral over a straight line in the z-direction, where $\alpha_\omega = 4\pi R^3\epsilon_0\left(\frac{\epsilon-1}{\epsilon+2}\right)$ is the polarizability of the sphere, I is the peak laser intensity, and τ is the pulse duration. After propagating to the grating over a time t_0, the sheared Wigner distribution w_1 transforms at the grating into a new Wigner fucntion w_2 via the integration kernel [33]

$$w_2(x, p; t_0) = \int_{-\infty}^{\infty} dp_0 dx_0 K(x, p; x_0, p_0) w_1(x_0, p_0; t_0), \tag{A2}$$

where

$$K(x, p; x_0, p_0) = \frac{1}{2\pi\hbar} \int ds\, ds_0\, e^{i(p_0 s_0 + ps)/\hbar} \langle x - s/2|U|x_0 + s_0/2\rangle \langle x + s/2|U^*|x_0 - s_0/2\rangle \tag{A3}$$

$$= \frac{1}{2\pi\hbar} \delta(x - x_0) \sum_{j,m\in\mathbb{Z}} b_j b_{j-m}^* e^{2\pi imx/d}$$

$$\times \delta\left(p - p_0 - (j - m/2)\frac{2\pi\hbar}{d}\right). \tag{A4}$$

The integration kernel K is obtained by transforming the wave function by the phase $\exp(i\phi(x))$ and plugging the transformed wave function into Eq. (A1) to obtain Eq. (A3). After Fourier expanding we obtain Eq. (A4). The $b_m = (-i)^m e^{i\phi_0/2} J_m(\phi_0/2)$ are called Talbot–Lau coefficients [46]. After propagating for an additional time t_1 to the detector, the final fringe pattern can be obtained by integrating the sheared distribution w_2 over momentum:

$$W_3(x) = |\psi_{CM}(x)|^2$$

$$= \int_{-\infty}^{\infty} dp\, w_2\left(x - \frac{p}{M} t_1 + \frac{1}{2} a t_1^2, p - Mat_1\right).$$

The final fringe pattern is a sum of wave packets weighted by the Bessel functions $b_j b_{j-m}^*$, each with spatial period

$$D \approx \frac{d}{m}\left(1 - \frac{t_1}{t_0 + t_1}\right)^{-1}. \tag{A5}$$

Because the b_m's decrease quickly as $|m|$ grows, to very good approximation, the period of the fringe pattern is that of the $m = 1$ term. So if the sphere falls for the same amount of time before and after interacting with the grating, $t_0 = t_1$ and $D \approx 2d$. This period is different from the period d which one normally associates with the Talbot effect, for example in the diffraction of beams of

molecules as in Ref. [46]. However, this result requires a position spread of the matter wave at the grating which is very large compared to the grating spacing. For the experimental parameters given in Table 1, by the time the sphere reaches the grating, its wave function has a position spread only of order the grating spacing. In the limit where the sphere falls for a very long time before reaching the grating, i.e. $t_0 \gg t_1$, its position spread would become large, and we would obtain from Eq. (A5) a period of $D \approx d$, as expected.

[1] A. Peters, K. Y. Chung, and S. Chu, Nature (London) **400**, 849 (1999); Metrologia **38**, 25 (2001).

[2] M. Kasevich and S. Chu, Phys. Rev. Lett. **67**, 181 (1991); Appl. Phys. B **54**, 321 (1992).

[3] H. Muller, S. W. Chiow, S. Herrmann, S. Chu, and K.-Y. Chung, Phys. Rev. Lett. **100**, 031101 (2008).

[4] J. M. McGuirk, G. T. Foster, J. B. Fixler, M. J. Snadden, and M. A. Kasevich, Phys. Rev. A **65**, 033608 (2002).

[5] T. L. Gustavson, P. Bouyer, and M. A. Kasevich, Phys. Rev. Lett. **78**, 2046 (1997).

[6] M. Prevedelli, L. Cacciapuoti, G. Rosi, F. Sorrentino, and G. M. Tino, Phil. Trans. R. Soc. A **372**, 0030 (2014).

[7] S. Dimopoulos and A. A. Geraci, Phys. Rev. D **68**, 124021 (2003).

[8] E. G. Adelberger, B. R. Heckel, and A. E. Nelson, Annu. Rev. Nucl. Part. Sci. **53**, 77 (2003).

[9] P. Wolf, P. Lemonde, A. Lambrecht, S. Bize, A. Landragin, and A. Clairon, Phys. Rev. A **75**, 063608 (2007).

[10] N. Arkani-Hamed, S. Dimopoulos, and G. Dvali, Phys. Lett. B **429**, 263 (1998).

[11] S. Dimopoulos and G. F. Guidice, Phys. Lett. B **379**, 105 (1996).

[12] G. Ferrari, N. Poli, F. Sorrentino, and G. M. Tino, Phys. Rev. Lett. **97**, 060402 (2006).

[13] J. Wacker, Phys. Lett. B **690**, 38 (2010).

[14] M. A. Naides, R. W. Turner, R. A. Lai, J. M. DiSciacca, and B. L. Lev, Appl. Phys. Lett. **103**, 251112 (2013).

[15] H. B. G. Casimir, Proc. K. Ned. Akad. Wet. **51**, 793 (1948).

[16] H. B. G. Casimir and P. Polder, Phys. Rev. **73**, 360 (1948).

[17] A. Canaguier-Durand, A. Gerardin, R. Guerout, P. A. Maia Neto, V. V. Nesvizhevsky, A. Yu. Voronin, A. Lambrecht, and S. Reynaud, Phys. Rev. A **83**, 032508 (2011).

[18] C. I. Sukenik, M. G. Boshier, D. Cho, V. Sandoghdar, and E. A. Hinds, Phys. Rev. Lett. **70**, 560 (1993).

[19] D. M. Harber, J. M. Obrecht, J. M. McGuirk, and E. A. Cornell, Phys. Rev. A **72**, 033610 (2005).

[20] M. S. Chapman, C. R. Ekstrom, T. D. Hammond, J. Schmiedmayer, B. E. Tannian, S. Wehinger, and D. E. Pritchard, Phys. Rev. A **51**, R14 (1995).

[21] A. D. Cronin, J. Schmiedmayer, and D. E. Pritchard, Rev. Mod. Phys. **81**, 1051 (2009).

[22] J. Bateman, S. Nimmrichter, K. Hornberger, and H. Ulbricht, Nat. Commun. **5**, 4788 (2014).

[23] A. A. Geraci, S. J. Smullin, D. M. Weld, J. Chiaverini, and A. Kapitulnik, Phys. Rev. D **78**, 022002 (2008).

[24] I. Antoniadis, N. Arkani-Hamed, S. Dimopoulos, and G. Dvali, Phys. Lett. B **436**, 257 (1998).

[25] D. B. Kaplan and M. B. Wise, J. High Energy Phys. 08 (2000) 037; T. Damour and A. M. Polyakov, Nucl. Phys. **B423**, 532 (1994).

[26] N. Arkani-Hamed, S. Dimopoulos, and G. Dvali, Phys. Rev. D **59**, 086004 (1999).

[27] N. Arkani-Hamed and S. Dimopoulos, Phys. Rev. D **65**, 052003 (2002).

[28] I. Marson and J. E. Faller, J. Phys. E **19**, 22 (1986).

[29] Y. Hadjar, P. F. Cohadon, C. G. Aminoff, M. Pinard, and A. Heidmann, Europhys. Lett. **47**, 545 (1999).

[30] G. Anetsberger, O. Arcizet, Q. P. Unterreithmeier, R. Rivière, A. Schliesser, E. M. Weig, J. P. Kotthaus, and T. J. Kippenberg, Nat. Phys. **5**, 909 (2009).

[31] J. Gieseler, B. Deutsch, R. Quidant, and L. Novotny, Phys. Rev. Lett. **109**, 103603 (2012).

[32] S. Nimmrichter, P. Haslinger, K. Hornberger, and M. Arndt, New J. Phys. **13**, 075002 (2011).

[33] S. Nimmrichter and K. Hornberger, Phys. Rev. A **78**, 023612 (2008).

[34] J. Chiaverini, S. J. Smullin, A. A. Geraci, D. M. Weld, and A. Kapitulnik, Phys. Rev. Lett. **90**, 151101 (2003).

[35] D. J. Kapner, T. S. Cook, E. G. Adelberger, J. H. Gundlach, B. R. Heckel, C. D. Hoyle, and H. E. Swanson, Phys. Rev. Lett. **98**, 021101 (2007).

[36] R. S. Decca, D. Lopez, E. Fischbach, G. L. Klimchitskaya, D. E. Krause, and V. M. Mostepanenko, Phys. Rev. D **75**, 077101 (2007).

[37] R. S. Decca, D. Lopez, H. B. Chan, E. Fischbach, D. E. Krause, and C. R. Jamell, Phys. Rev. Lett. **94**, 240401 (2005).

[38] M. Masuda and M. Sasaki, Phys. Rev. Lett. **102**, 171101 (2009).

[39] S. K. Lamoreaux, Phys. Rev. Lett. **78**, 5 (1997).

[40] A. O. Sushkov, W. J. Kim, D. A. R. Dalvit, and S. K. Lamoreaux, Phys. Rev. Lett. **107**, 171101 (2011).

[41] G. Ranjit, D. P. Atherton, J. Stutz, M. Cunningham, and A. A. Geraci, Phys. Rev. A **91**, 051805(R) (2015).

[42] D. C. Moore, A. D. Rider, and G. Gratta, Phys. Rev. Lett. **113**, 251801 (2014).

[43] C. C. Speake and C. Trenkel, Phys. Rev. Lett. **90**, 160403 (2003).

[44] R. O. Behunin, D. A. R. Dalvit, R. S. Decca, and C. C. Speake, Phys. Rev. D **89**, 051301(R) (2014).

[45] A. Lambrecht and S. Reynaud, Eur. Phys. J. D **8**, 309 (2000).

[46] K. Hornberger, S. Gerlich, H. Ulbricht, L. Hackermuller, S. Nimmrichter, I. V. Goldt, O. Boltalina, and M. Arndt, New J. Phys. **11**, 043032 (2009).